Supplementary data

Aqua Coordination to Attenuate the Luminescence Properties of Europium(III)-Phosphine Oxide Porous Coordination Polymers

Kosuke Katagiri,*, † Naoya Matsuo, † Masatoshi Kawahata, ‡ Hyuma Masu,§ and Kentaro Yamaguchi ‡

Table of Contents

NMR Spectroscopy

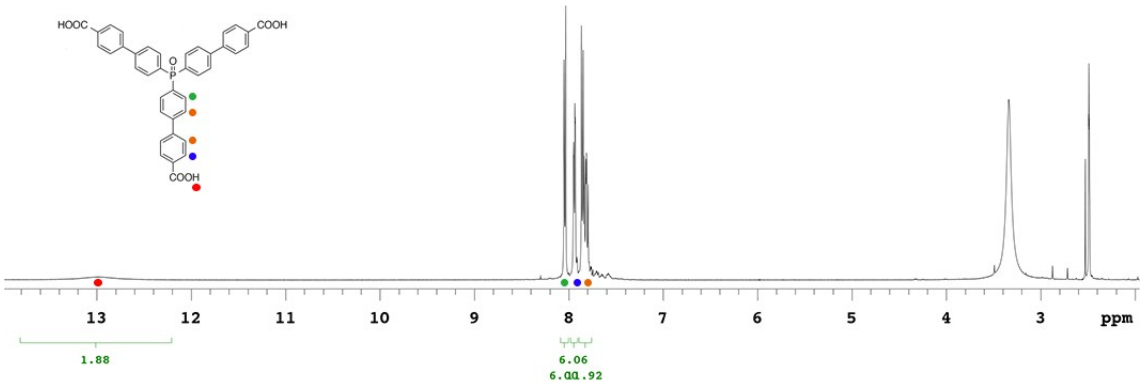

Fig. S1. ^{1}H NMR of **1** in $CDCl_3$.

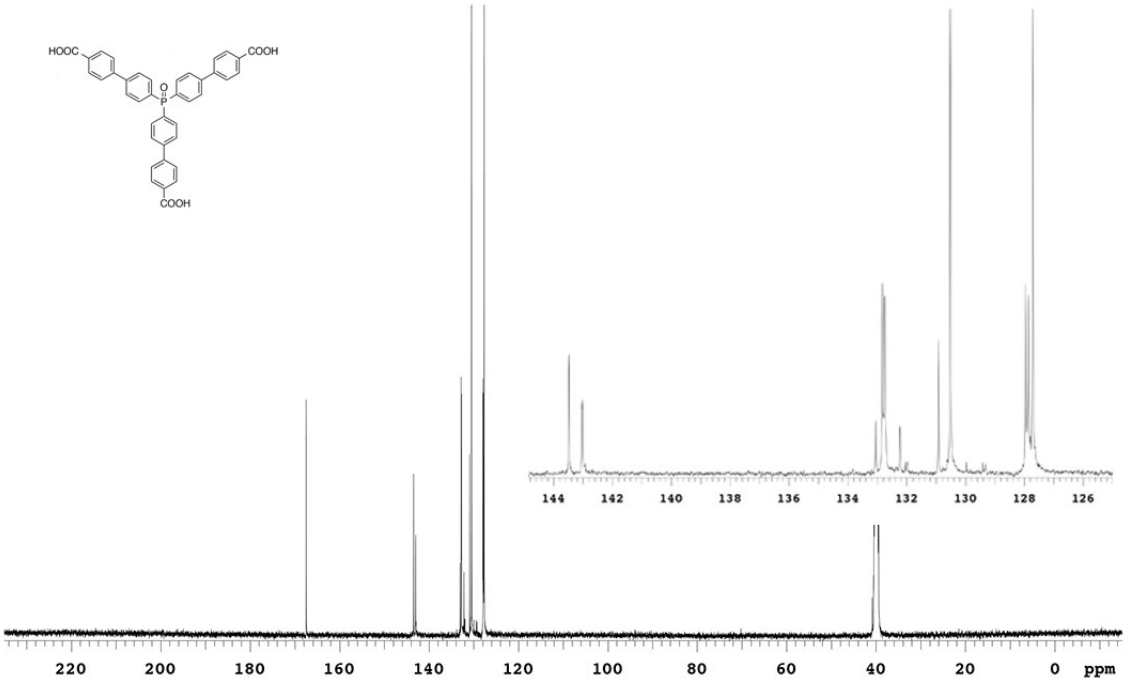

Fig. S2. ^{13}C NMR of **1** in $CDCl_3$.

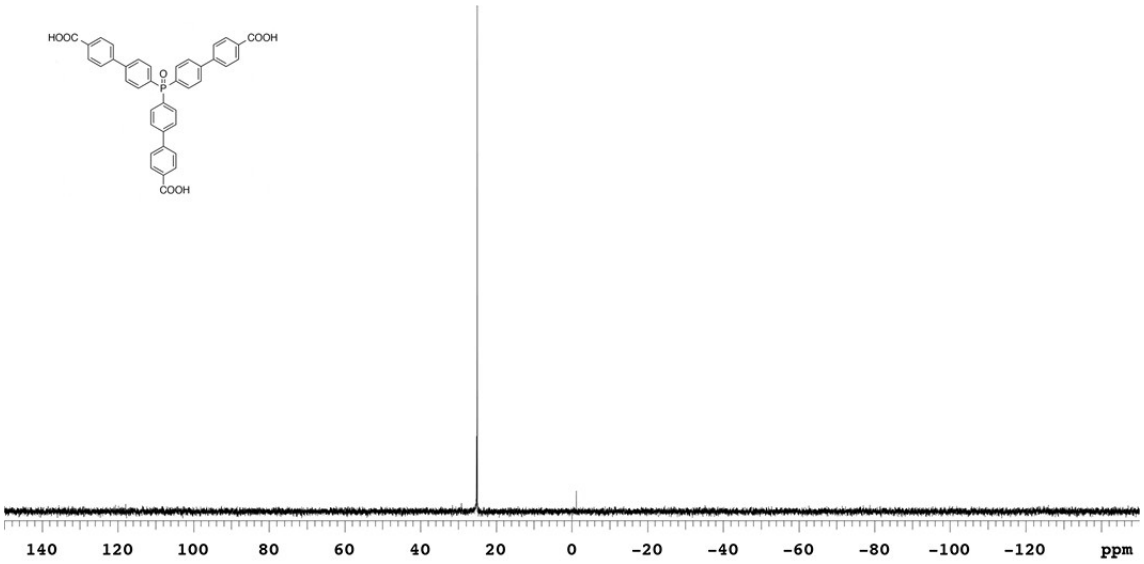

Fig. S3. ^{31}P NMR of **1** in $CDCl_3$.

ESI-MS Spectroscopy

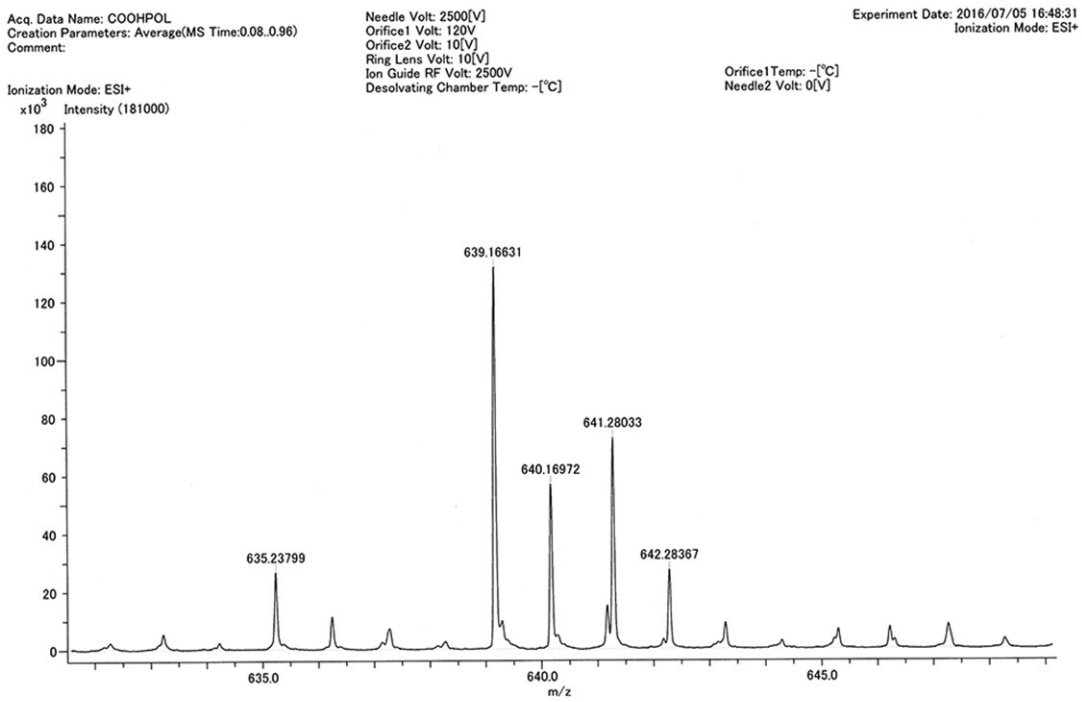

Fig. S4. ESI-MS spectrum of **1** in DMSO/MeOH.

Thermogravimetric Analysis

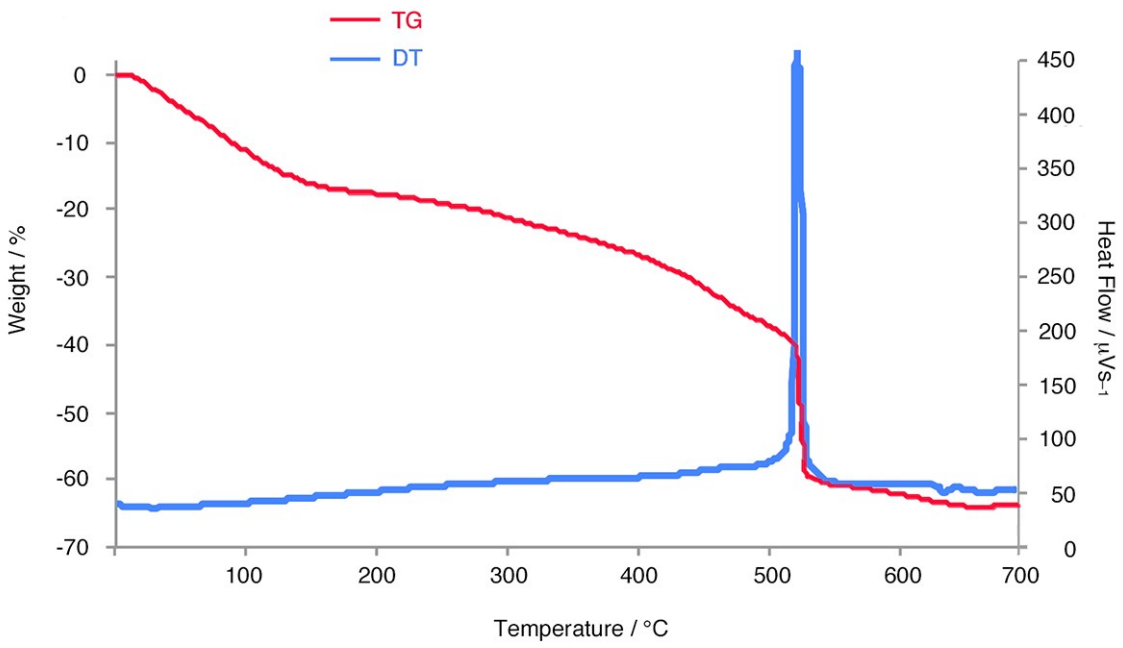

Fig. S5. TGA curve for as-synthesized [Eu(**1**)·dmf]$_n$ (**1a**).

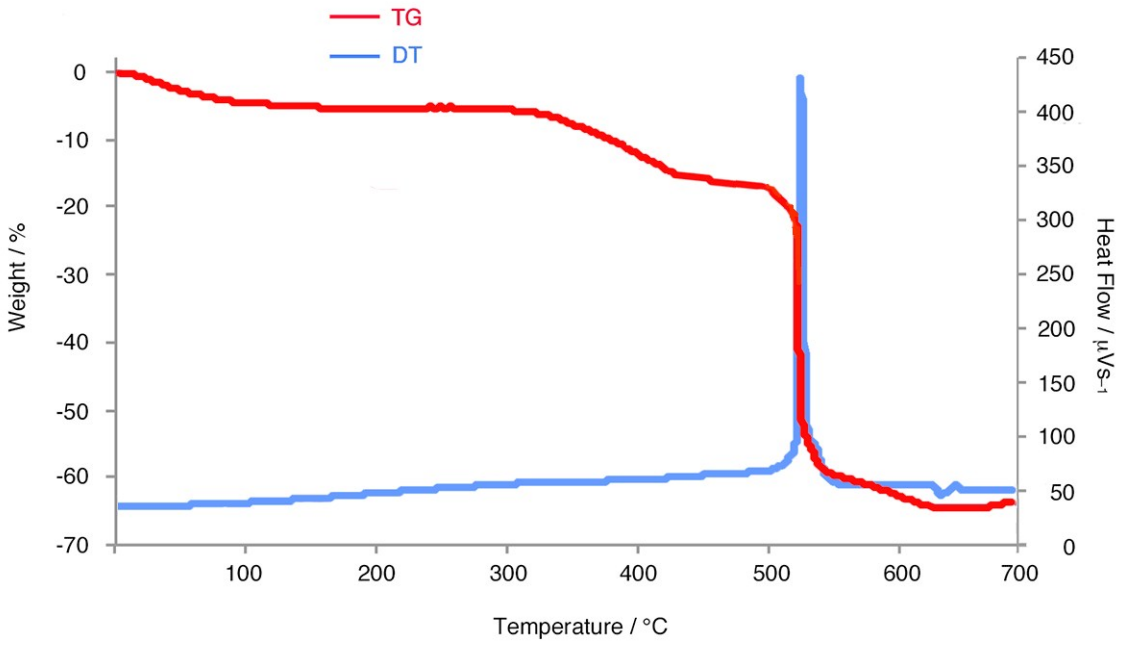

Fig. S6. TGA curve for desolvated [Eu(**1**)·dmf·h_2o]$_n$ (**1a**).

Luminescence Property

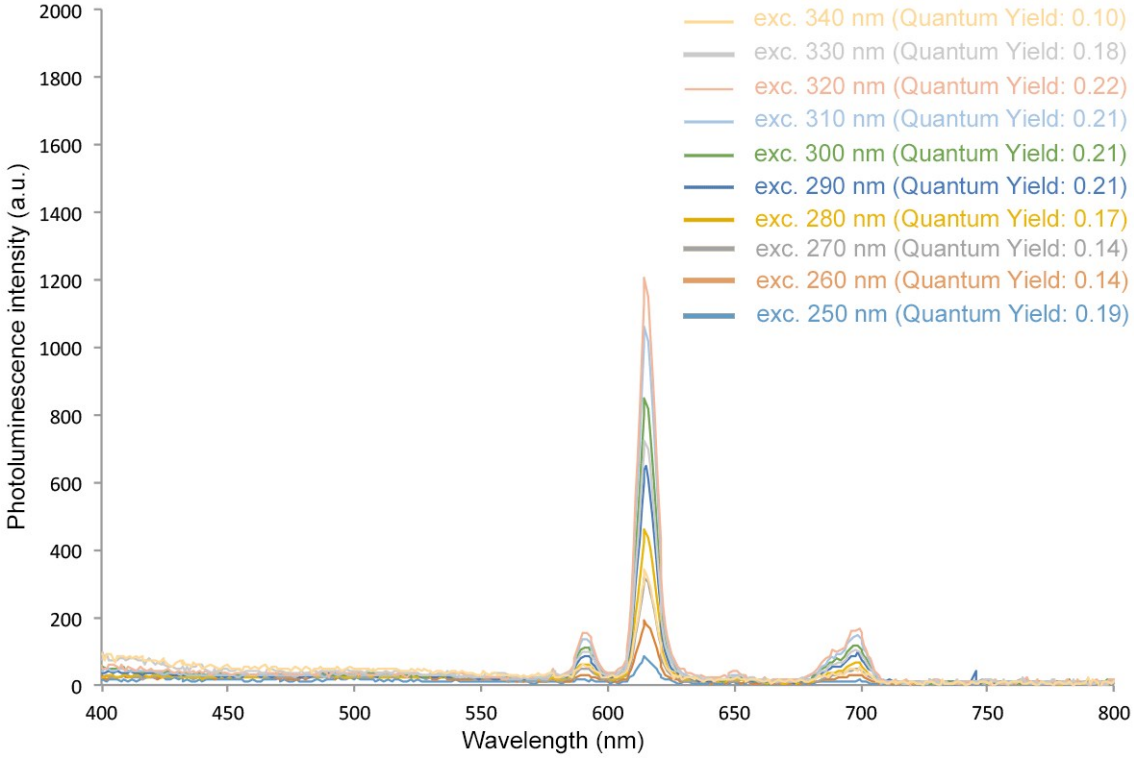

Fig. S7. Solid-state emission spectra of $[Eu(\mathbf{1})\cdot dmf]_n$ (**1a**).

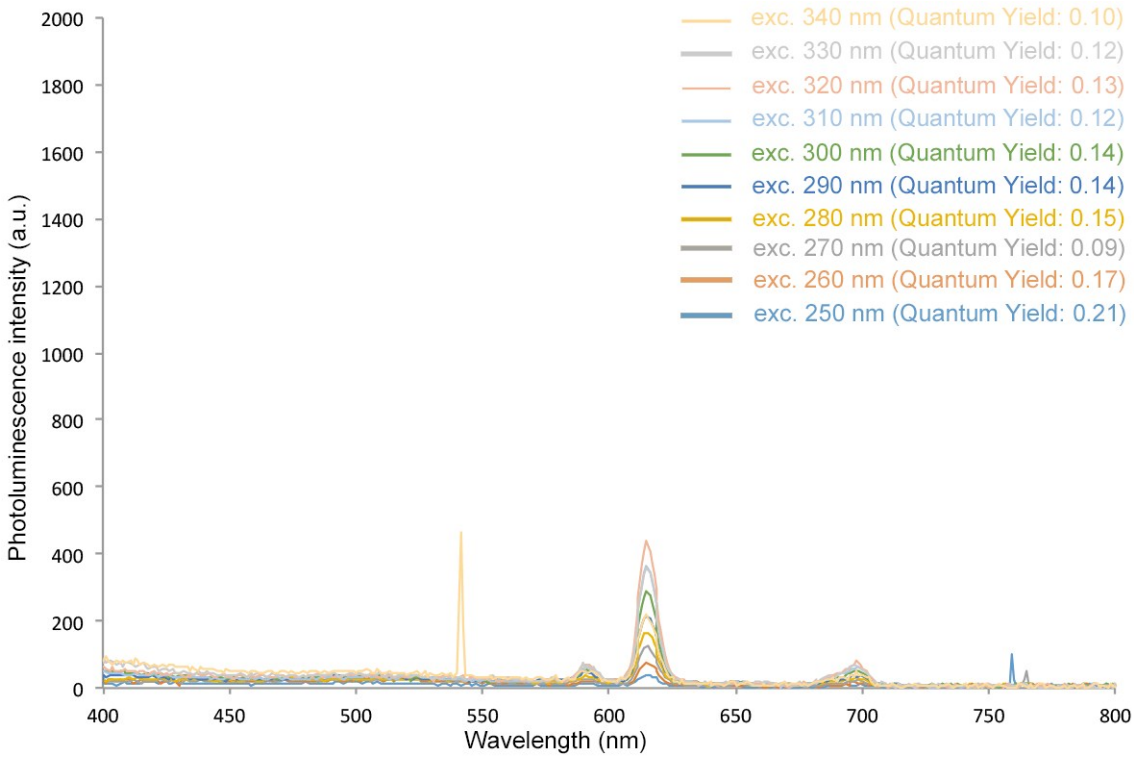

Fig. S8. Solid-state emission spectra of $[Eu(\mathbf{1})\cdot dmf\cdot H_2O]_n$ (**1b**).

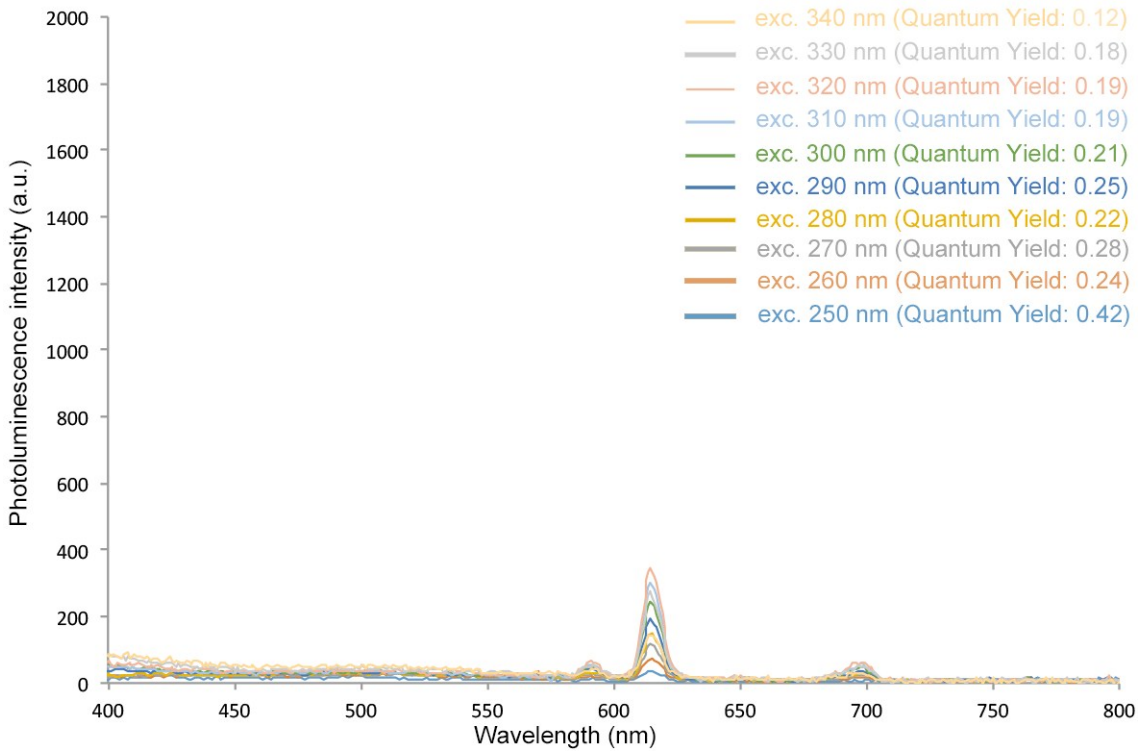

Fig. S9. Solid-state emission spectra of [Eu(**1**)· $H_2O]_n$ (**1c**).

Powder X-ray Diffraction Pattern

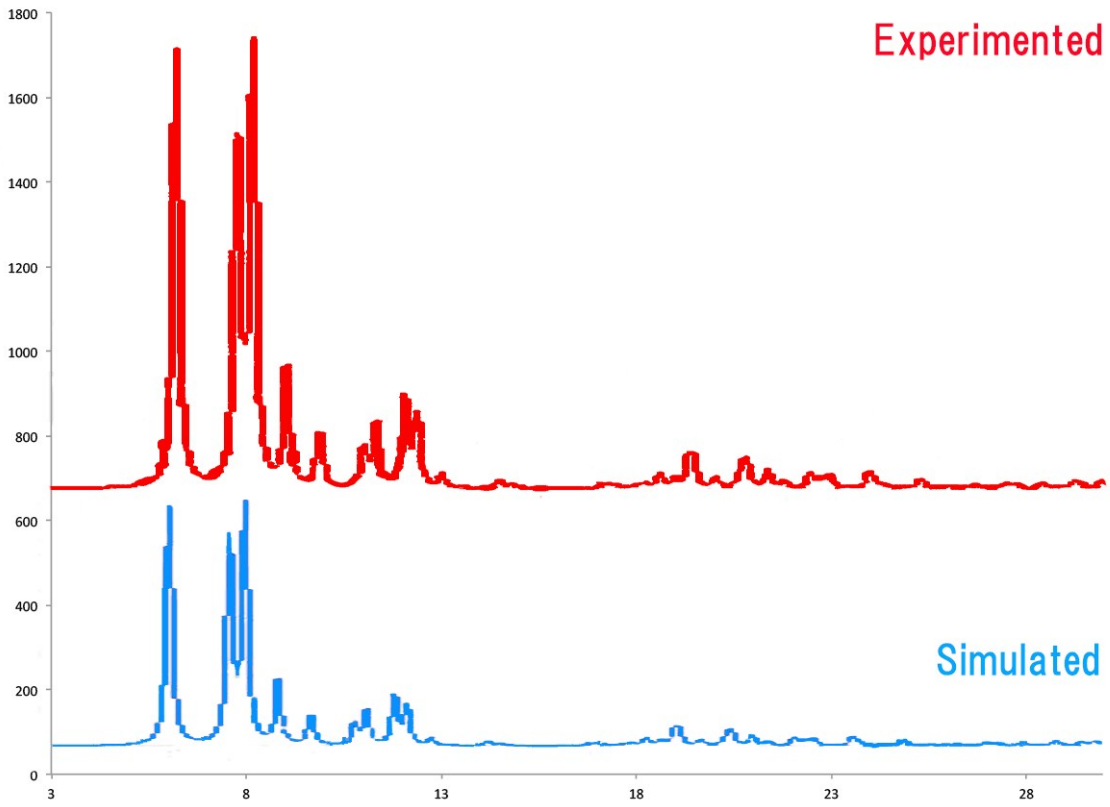

Fig. S10. PXRD pattern for [Eu(**1**)·dmf]$_n$ (**1a**).

X-ray Crystallographic Analysis

Table S1. Crystal data of [Eu(**1**)·dmf]$_n$ (**1a**) and [Eu(**1**)·dmf·H_2O]$_n$ (**1b**).

	[Eu(**1**)·dmf]$_n$ (**1a**)	[Eu(**1**)·dmf·H_2O]$_n$ (**1b**)
formula	$C_{42}H_{31}NO_8PEu$	$C_{40.64}H_{27.82}N_{0.55}O_8PEu$
formula weight	860.61	834.76
T (K)	273	273
crystal system	orthorhombic	orthorhombic
space group	*Pcca*	*Pcca*
a (Å)	36.202(7)	36.205(7)
b (Å)	15.391(3)	15.379(3)
c (Å)	29.655(6)	29.692(6)
α (°)	90	90
β (°)	90	90
γ (°)	90	90
V (Å^3)	16523(6)	16532(6)
Z	8	8
D_{calc} (gm^{-3})	0.692	0.671
μ (mm^{-1})	1.088	1.086
F(000)	3456	3340
θ range (deg)	1.793–35.397	1.794–32.028
no. of reflections collected	45205	35578
no. of unique reflections (R_{int})	23666 (0.0474)	18374 (0.0124)
goodness of fit on F^2	0.718	1.094
R_1, wR_2 [$I > 2\sigma(I)$]	0.0515, 0.1599	0.0428, 0.1318
R_1, wR_2 (all data)	0.0661, 0.1798	0.0515, 0.1378
CCDC number	CCDC-1486160	CCDC-1486159

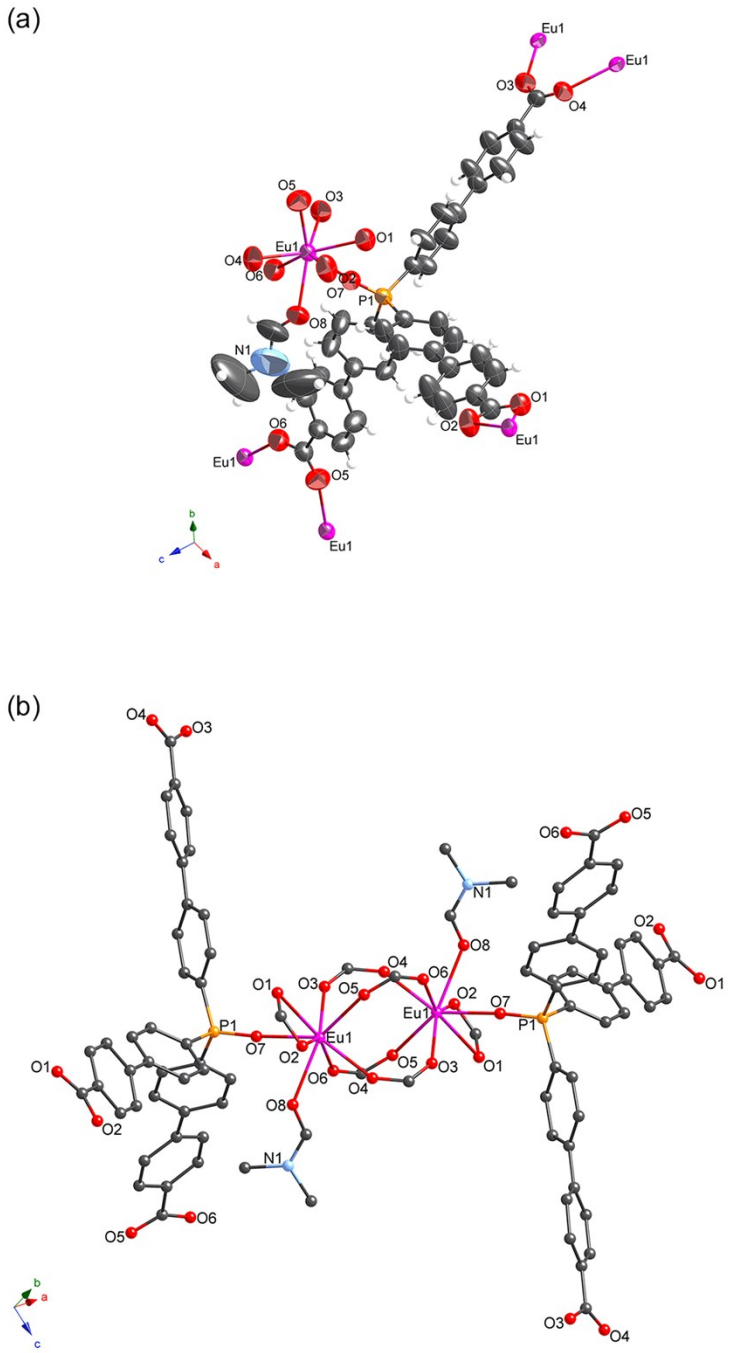

Fig. S11. (a) Asymmetric unit of [Eu(**1**)·dmf]$_n$ (**1a**) in the thermal ellipsoid model. The ellipsoids of all non-hydrogen atoms have been drawn at the 50% probability level. (b) Dinuclear metal center coordinated with eight ligands and two DMF molecules.

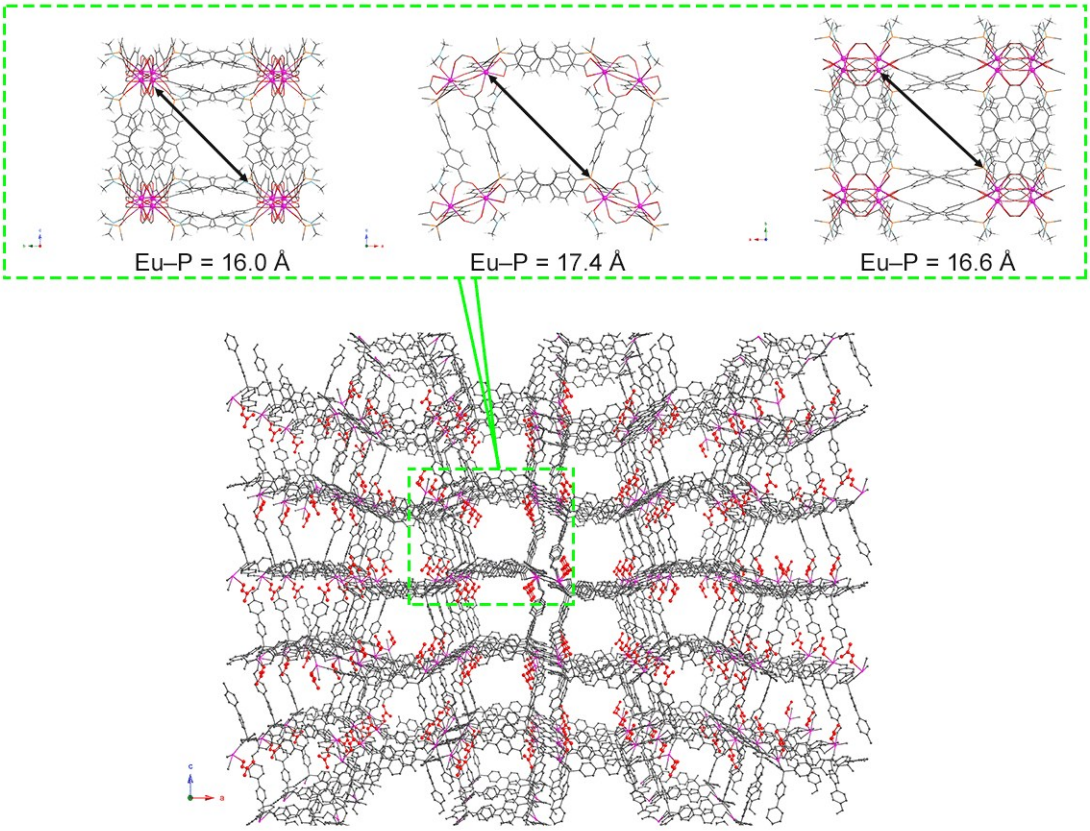

Fig. S12. Ball and stick model of 3D framework of [Eu(**1**)·dmf]$_n$ (**1a**). Insets: View of the open pore along *a* axis (left), *b* axis (center) and *c* axis (right).

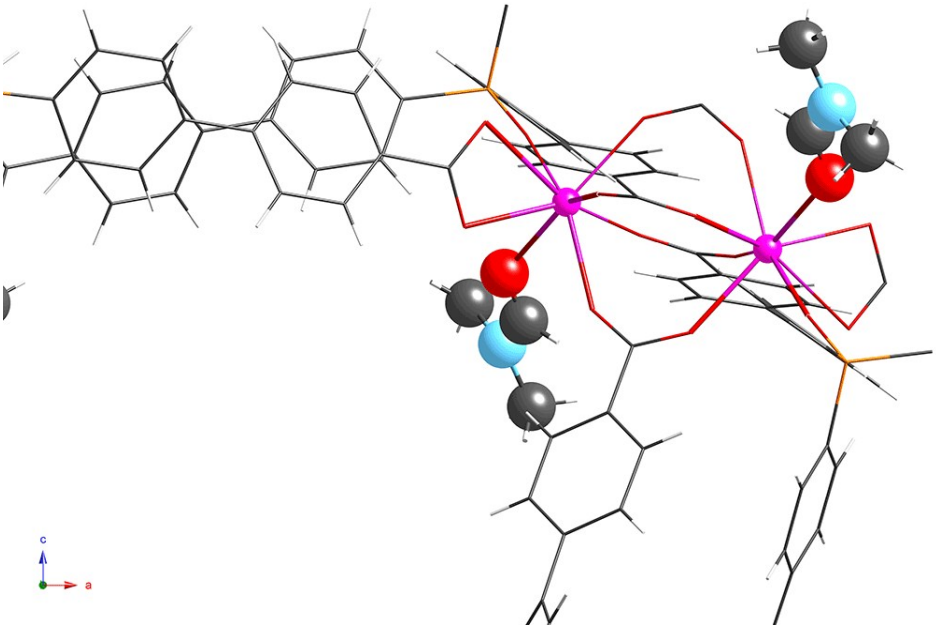

Fig. S13. View of the Eu(III) coordination sphere of [Eu(**1**)·dmf]$_n$ (**1a**).

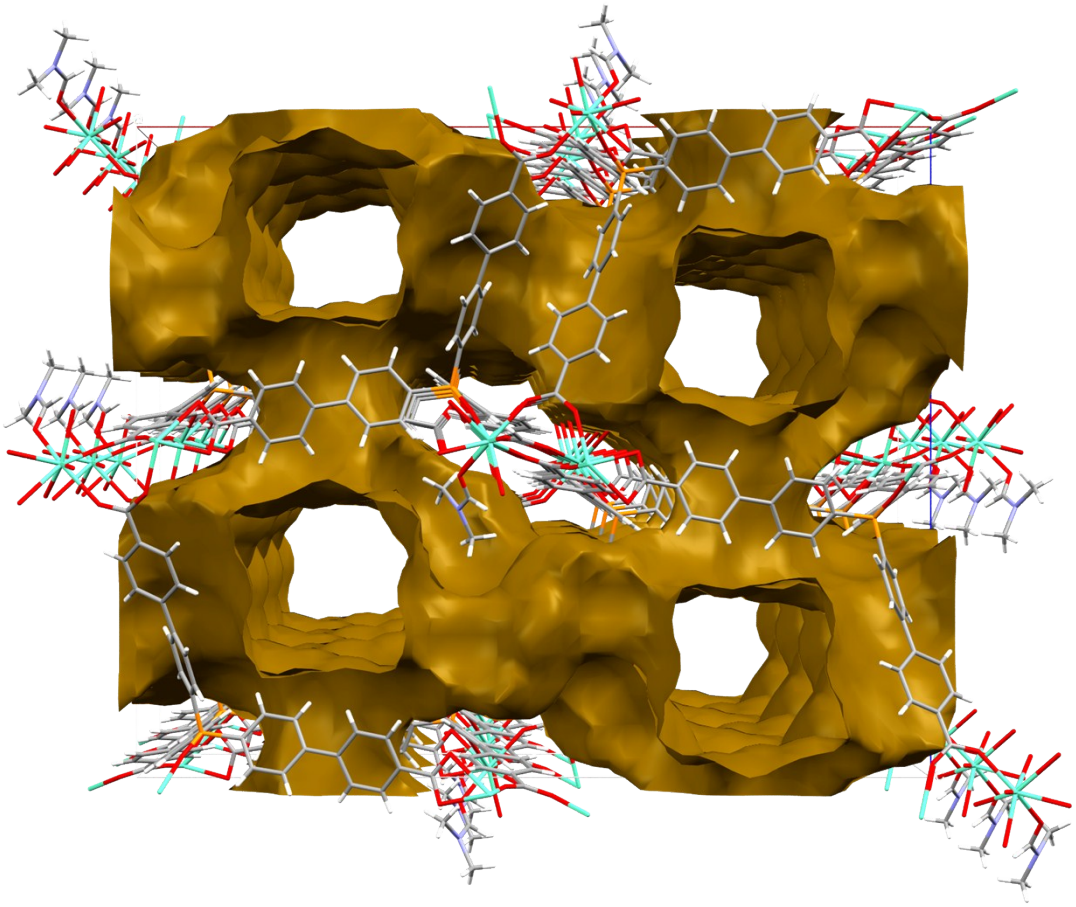

Fig. S14. Solvent-accessible voids of [Eu(**1**)·dmf]$_n$ (**1a**) in the *ac* plane.

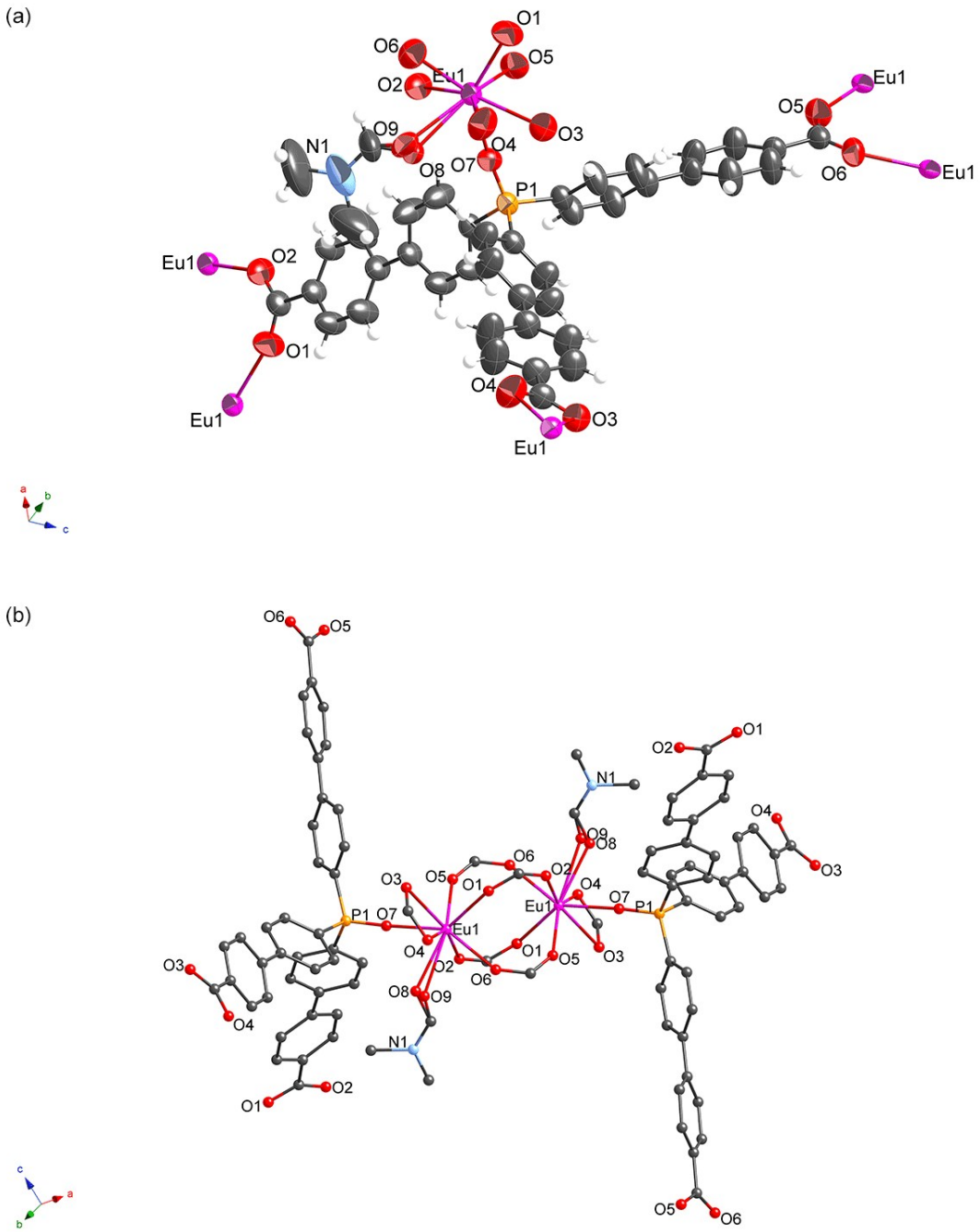

Fig. S15. (a) Asymmetric unit of $[Eu(\mathbf{1})\cdot 0.55dmf\cdot 0.45H_2O]_n$ (**1b**) in the thermal ellipsoid model. The ellipsoids of all non-hydrogen atoms have been drawn at the 50% probability level. (b) Dinuclear metal center coordinated with eight ligands and two DMF/H_2O molecules.

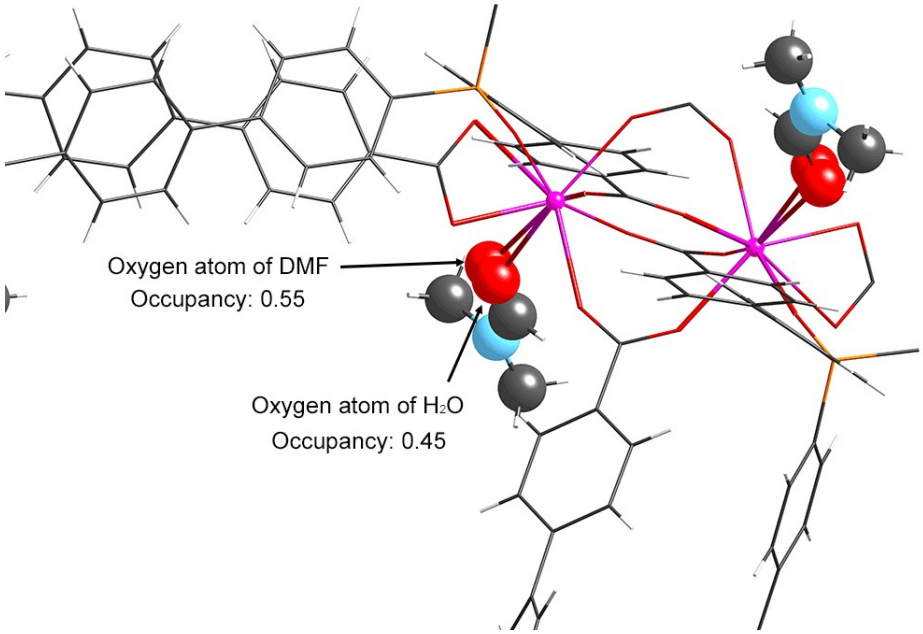

Fig. S16. View of the Eu(III) coordination sphere of [Eu(**1**)·0.55dmf·0.45H_2O]$_n$ (**1b**).

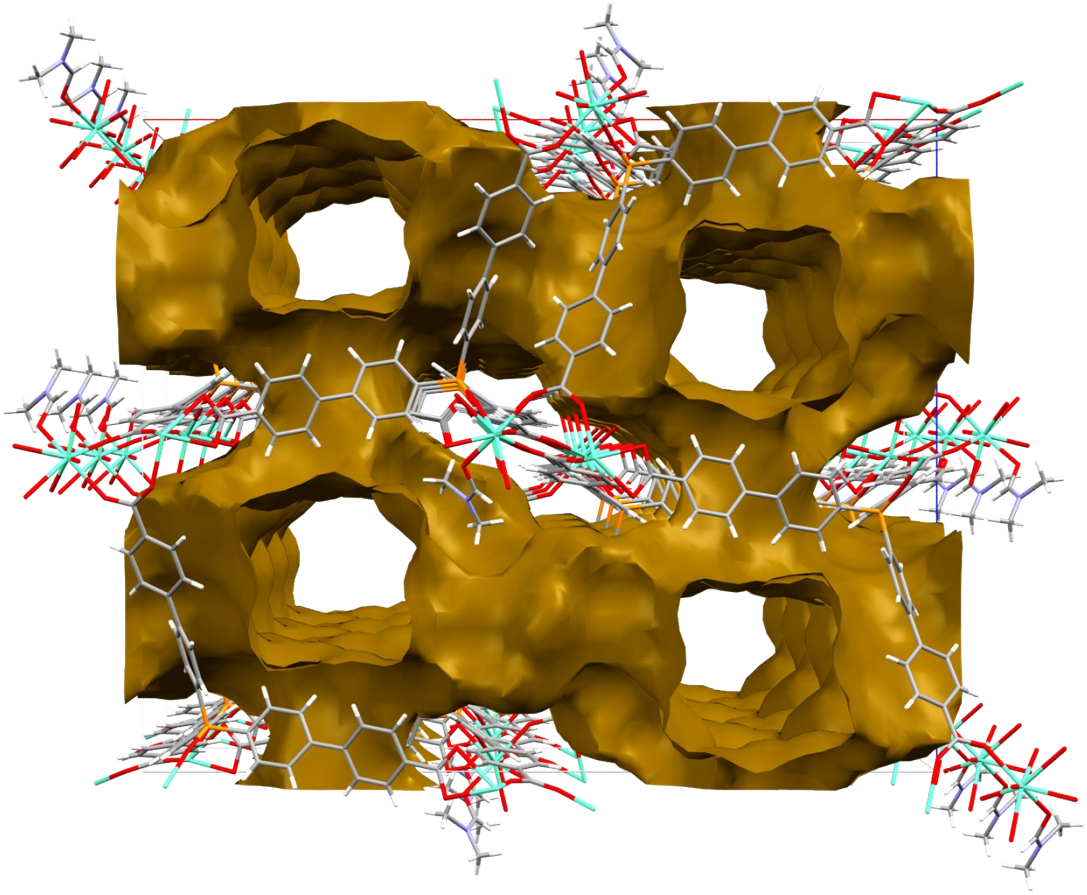

Fig. S17. Solvent-accessible voids of [Eu(**1**)·0.55dmf·0.45H_2O]$_n$ (**1b**) in the *ac* plane.

Adsorption-Desorption Isotherms

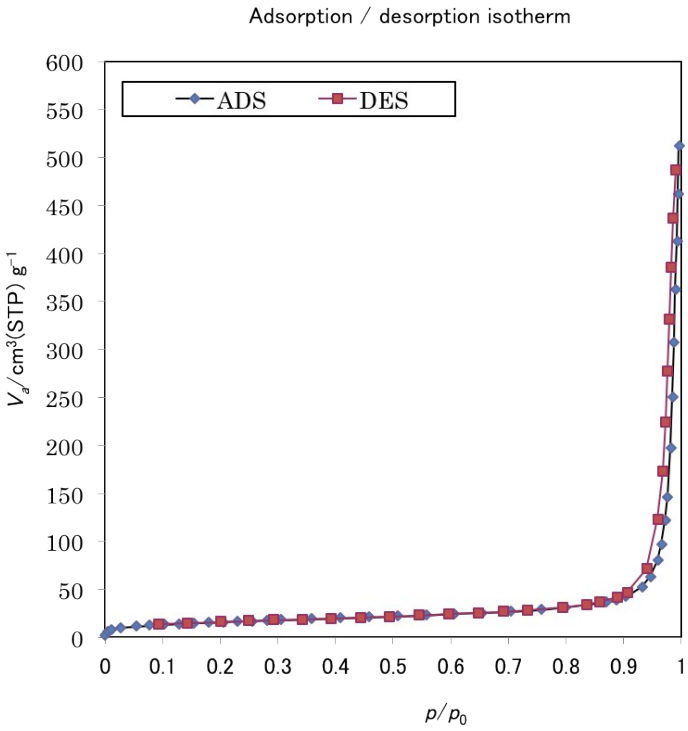

Fig. S18. Adsorption-desorption isotherm for [Eu(**1**)·dmf] (**1a**)

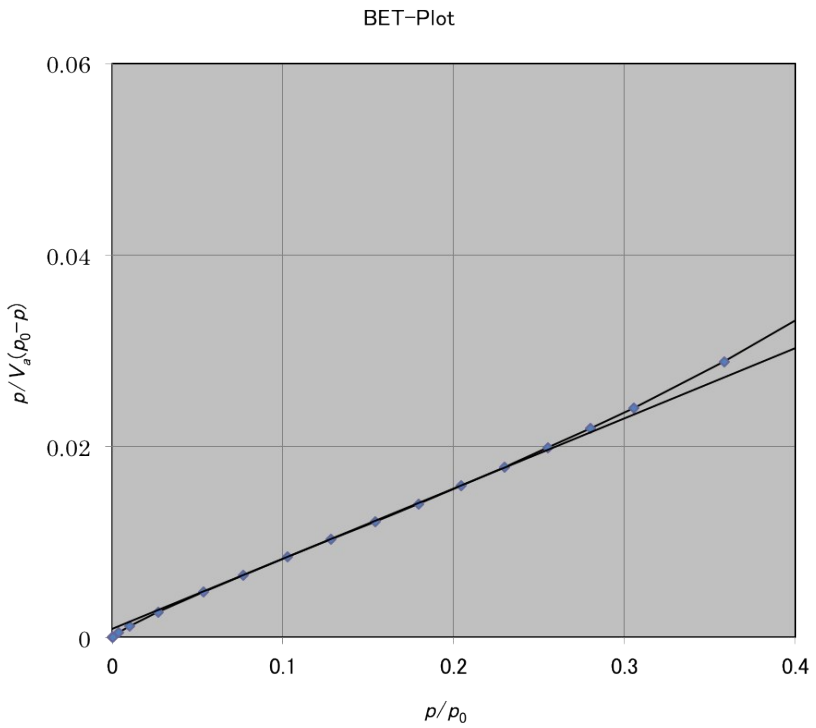

Fig. S19. BET-Plot for [Eu(**1**)·dmf] (**1a**)

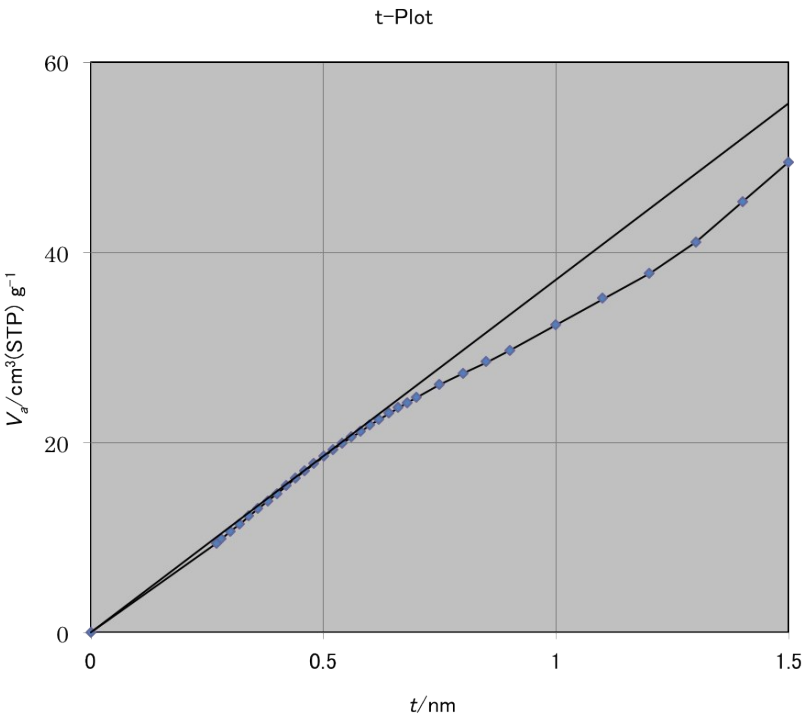

Fig. S20. t-Plot for [Eu(**1**)·dmf] (**1a**)

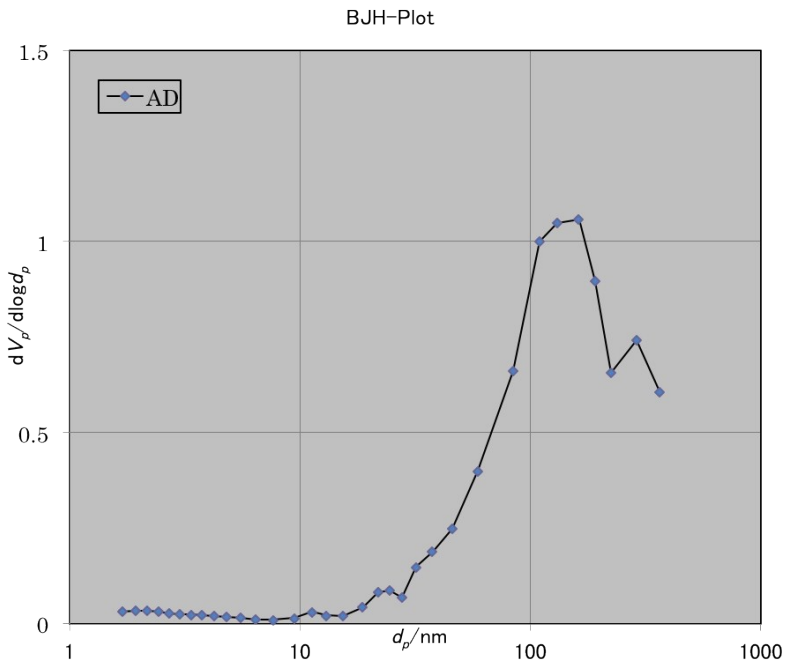

Fig. S21. BJH(ads)-Plot for [Eu(**1**)·dmf] (**1a**)

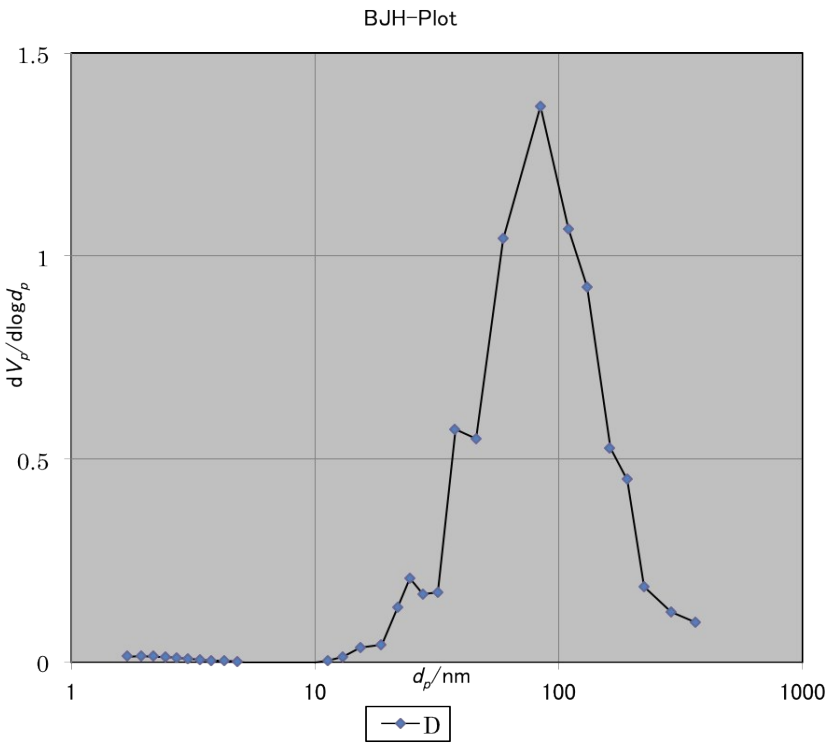

Fig. S22. BJH(des)-Plot for [Eu(**1**)·dmf] (**1a**)